H2S removal from syngas using wastes pyrolysis chars

Maxime Hervy, Doan Pham Minh, Claire Gerente, Elsa Weiss-Hortala, Ange Nzihou, Audrey Villot, Laurence Le Coq

H_2S removal from syngas using wastes pyrolysis chars

Maxime Hervy[a,b,*], Doan Pham Minh[a], Claire Gérente[b], Elsa Weiss-Hortala[a], Ange Nzihou[a], Audrey Villot[b], Laurence Le Coq[b]

[a] Université de Toulouse, Mines Albi, CNRS, Centre RAPSODEE, Campus Jarlard, Route de Teillet, F.81013 Albi Cedex09, France
[b] IMT Atlantique, GEPEA UMR CNRS 6144, Université Bretagne Loire, 4 rue A. Kastler, CS 20722, 44307 Nantes Cedex 03, France

GRAPHICAL ABSTRACT

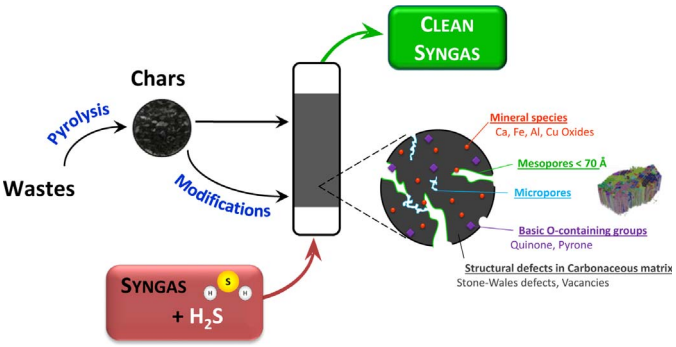

Keywords:
Activated carbon
Adsorption
Biochar
Desulfurization
Gas cleaning
Waste valorization

ABSTRACT

Pyrolysis chars from wastes were investigated as sorbents for H_2S removal from syngas. The H_2S removal tests were performed at ambient temperature in various dry gas matrices (N_2, Air, Syngas) to study the effect of the gas composition on the adsorption efficiency. Two chars were produced by the pyrolysis of: used wood pallets (UWP), and a 50/50% mixture of food waste (FW) and coagulation-flocculation sludge (CFS). The chars were functionalized by low-cost processes without chemicals: gas phase oxygenation and steam activation. Activated chars were the most efficient materials due to their large specific surface area, alkaline pH, basic O-containing groups and structural defects in graphene-like sheets. Raman analysis evidenced that inherent mineral species (especially Ca and Fe) increased the H_2S removal efficiency by promoting the formation of metal sulfide and metal sulphate species at the char surface. Mesopores lower than 70 Å were revealed to be important adsorption sites. Under dry Syngas matrix, the chars remained efficient and selective toward H_2S removal despite the presence of CO_2, while O_2 in the Air matrix decreased their removal capacity due to the formation of sulfur acid species. The most efficient material was the steam activated char from FW/CFS, with a removal capacity of 65 $mg_{H2S}.g^{-1}$ under dry syngas. This char was proved to be completely regenerated with a thermal treatment under N_2 at 750 °C. This study demonstrated that activated chars from food waste and sludge could be used as eco-friendly, affordable, and selective materials for syngas desulfurization even under dry atmosphere.

Abbreviations: UWP, Used Wood Pallets; FW, Food Waste; CFS, Coagulation-Flocculation Sludge; S_{BET}, specific surface area (in $m^2.g^{-1}$); Q_{remov}, H_2S removal capacity of the adsorbent (in $mg_{H2S}.g^{-1}$); wt%, percentage by weight; v%, percentage by volume; HK, Horvath-Kawazoe, method used to calculate the microporous volume; BJH, Barrett Joyner et Halenda method used to calculate the mesoporous volume

* Corresponding author at: Université de Toulouse, Mines Albi, CNRS, Centre RAPSODEE, Campus Jarlard, Route de Teillet, F.81013 Albi Cedex09, France.
E-mail addresses: maxime.hervy@mines-albi.fr (M. Hervy), doan.phamminh@mines-albi.fr (D. Pham Minh), claire.gerente@imt-atlantique.fr (C. Gérente), elsa.weiss@mines-albi.fr (E. Weiss-Hortala), ange.nzihou@mines-albi.fr (A. Nzihou), audrey.villot@imt-atlantique.fr (A. Villot), laurence.le-coq@imt-atlantique.fr (L. Le Coq).

1. Introduction

Pyrogasification is an efficient process to convert a large variety of wastes generated by modern societies into energy [1]. Feedstock, such as waste or biomass, is degraded under controlled temperature and atmosphere [2]. Char, tar, and synthesis gas (syngas) are the main products of this process, and their yields depend on the nature of the feedstock and the operating conditions. Pyrolysis chars represent typically 15–30 wt% of the feedstock. Nowadays, chars are considered as wastes and the additional costs required for their disposal decrease the economic viability of the pyrogasification process. For this reason, new routes for char valorization are studied: soil amendment and fertilizer [3], sorbent for water treatment [4] and gas cleaning [5], catalyst [6,7] and catalyst support [8] for gas treatment. The syngas produced by pyrogasification is mainly composed of permanent gases, such CO, H_2, CO_2, CH_4 and small hydrocarbons (C_2-C_3). Syngas can be used in many applications depending on its purity: combustible in gas engine, gas turbine or fuel cell to generate power and heat; precursor for liquid fuel and chemicals synthesis [9]. The sulfur content of the feedstock leads to the formation of hydrogen sulfide (H_2S) in the syngas, usually ranging from 100 to 200 ppmv [10] but possibly reaching 3.5% [11]. H_2S must be removed in order to avoid the corrosion of metal surfaces, the poisoning of costly catalysts used for syngas upgrading (mainly Fe- and Ni-based catalysts), and the generation of sulfur dioxide (if combusted), a major contributor to acid rain [9].

Several adsorbents have been studied for gas desulfurization, such as zeolites [12], activated carbon [13], and metal oxides (zinc, cobalt, iron) dispersed on various supports: mesoporous silica [14–16], graphite oxides [17–19], hydroxyapatite [20], and functionalized activated carbon [21,22]. Most of the studies dealing with gas desulfurization at room temperature using activated carbon were focused on H_2S removal from moist air. In the presence of oxygen and humidity, the interactions between H_2S and the complex surface properties of the activated chars (O-containing groups, mineral species, pH) lead to several retention mechanisms including dissociative adsorption and oxidation [23–26]. High specific surface areas and large microporous volumes are also known to promote the purification efficiency of the chars [13]. Usually, the conditions of char's production are adjusted in order to obtain materials with suitable properties [27]. Special modifications using chemicals, such as caustic impregnations or activation [28–30] and metal impregnation [21,22,31–34] are carried out to enhance the activated carbon efficiency. However, these processes have high environmental footprint (use and management of chemicals), increase the cost of the materials and jeopardize their regeneration (low temperature of self-ignition) [35].

Few studies compared the H_2S removal efficiency of activated carbon in moist and dry conditions and revealed that humidity strongly promoted the adsorption efficiency of activated carbon [5,24,36]. The reaction mechanism in dry atmosphere with zeolite has recently been investigated [12], but still remains unclear with activated carbons. Thus, an improvement of the sulfur products identification is needed to better understand the complex reactive-adsorption mechanism involved without humidity. In addition, the use of carbonaceous materials for syngas desulfurization at ambient temperature has, to the best of our knowledge, never been studied. Some researchers worked on H_2S removal from biogas and highlighted that the presence of CO_2 in the gas matrix negatively affected the activated carbons efficiency due to competitive effects with H_2S [21,32]. As CO_2 concentration in the syngas ranges from 5 to 20%, similar phenomenon can be observed.

The aim of this work is to study the performance of waste-based chars as low-cost adsorbents for the H_2S removal in dry syngas at ambient temperature. The objectives were to better understand the relationships between the materials performance in several dry gas matrices and: (1) the physicochemical properties of the chars, and (2) the speciation of the sulfur compounds adsorbed. Three abundant wastes generated on cruise ships were used – namely used wood pallets (UWP), food waste (FW), and coagulation-flocculation sludge (CFS). The annual generation in France was 6.2 Mt for wood waste in 2012, 9.0 Mt for sludge in 2013, and 7.1 Mt for food waste in 2013 [37]. To study the influence of the chemical composition of the chars on their H_2S removal performances, two pyrolysis chars were produced from different feedstocks. A carbonaceous char (c.UWP) was produced from UWP, and a char rich in minerals (c.FW/CFS) was produced from a mixture of 50 wt % FW and 50 wt% CFS. In addition, these mixtures were selected as mineral waste and wood waste are two different streams that require separate treatment process. An important aspect of this study consists in the choice of eco-friendly, sustainable, and low-cost processes for the production and the improvement of the chars. A short time pyrolysis (30 min) compared to usual carbonization processes (up to few hours [1]) was conducted and the resulting chars were modified by two processes without any chemicals: gas phase oxygenation and steam activation. The adsorption tests were not "accelerated" by the use of excessively high H_2S concentrations, in order to avoid kinetic limitations and misleading interpretation [24]. Furthermore, the influence of the gas composition was investigated using three different gas mixtures containing 200 ppmv of H_2S (Nitrogen, Air, and model Syngas composed of H_2, CO, CO_2, CH_4 and N_2). A special attention was paid for the identification of the sulfur compounds speciation to better understand the reaction mechanism in dry atmosphere. The regeneration capacity of the samples, which is a key point for their industrial utilization [38], was also explored.

2. Materials and methods

2.1. Char production and modification

2.1.1. Raw materials

The waste materials used in this study were from cruise ships: Used Wood Pallets (UWP), Food Waste (FW) and Coagulation-Flocculation Sludge (CFS). UWP was common softwood (from gymnosperm trees) used in the production of pallets for loading and transportation of food. Food wastes came from feeding activity, and were composed of a mixture of vegetables and animal wastes. Coagulation-Flocculation Sludge was recovered from a wastewater treatment plant present on board. FW and CFS were partially dehydrated in a screw press up to a moisture content of 80 wt%, and dried up to a moisture of 30 wt% in a steam dryer (Scanship). Before pyrolysis, these wastes were stored in closed bags. UWP was chipped in particles of average diameter of 3 cm and stored indoors. Based on these wastes, different chars were produced and two modifications were applied to the pyrolysis chars.

2.1.2. Pyrolysis treatment

The pyrolysis was performed at 700 °C during 30 min with a heating rate of 22 °C.min^{-1}, in a semi-continuous horizontal screw reactor (i.d. of 0.167 m and 2 m in length). Details of the experimental procedure were described elsewhere [39]. Two different pyrolysis chars were produced: (1) c.UWP, only from UWP, and (2) c.FW/CFS, from a mixture of 50 wt% FW and 50 wt% CFS. Prior to further utilization or characterization, the chars were sieved to particle size from 0.5 to 1.6 mm to avoid preferential pathways in the H_2S removal experiments.

2.1.3. Oxygenation of the pyrolysis chars by O_2/N_2 gas-phase treatment

An O_2/N_2 gas-phase treatment was performed in order to increase the amount of oxygenated groups on the char surface. The two pyrolysis chars were oxygenated in a fixed-bed vertical quartz reactor (internal diameter of 2.4 cm) placed in an electric furnace (Heraeus D-6450). The dry chars were loaded in the reactor (bed height of 15 cm) and heated to the oxygenation temperature (280 °C) under pure nitrogen with a heating rate of 20 °C.min^{-1}. Once the oxygenation temperature was reached, the nitrogen flow was replaced with a mixture of 8 v% O_2/92 v % N_2 at a flow rate of 2.0 L.min^{-1}. Previous study [40] and preliminary tests were performed to determine the optimal conditions of

oxygenation (temperature, duration). The pyrolysis chars were oxygenated at 280 °C during 4 h for c.UWP, and only 2 h for c.FW/CFS in order to limit the mass loss due to the combustion/gasification reactions catalysed by the large amount of mineral species contained in this char. The solid yield of this treatment was 97 wt% for ox.FW/CFS and 98 wt% for ox.UWP. After the oxygenation, the chars were named with the prefix "ox".

2.1.4. Steam activation of the pyrolysis chars

The pyrolysis chars were activated with steam, as this process is known to develop micro, meso and macropores [41,42]. Approximatively 100 g of pyrolysis char were introduced in a semi-rotation reactor in quartz (Carbolite HTR 11/150), and heated to 850 °C under inert atmosphere (N_2 flow) with a heating rate of 10 °C.min^{-1}. Once this temperature was reached, steam was added to the nitrogen flow at a concentration of 15 v%. The activation process was carried-out under these conditions for 80 min. The activated chars were named with the prefix "ac". The solid yield of this treatment was 69 wt% for ac.FW/CFS and 77 wt% for ac.UWP.

The materials were stored in closed bags and were not pretreated (dried or humidified) before the H_2S removal tests.

2.2. H_2S abatement experiments

The H_2S removal tests were performed in a glass fixed-bed reactor (14 mm i.d.) at room temperature (21–23 °C) (Fig. S1). The height of the fixed-bed char was set at 2.35 cm in order to reproduce a residence time in empty column (1.2 s) close to that of industrial processes (0.1–5 s) [43]. The gas velocity in empty column was 1.95 cm/s, which was lower than usual velocity in industrial processes (14–17 cm/s) [43]. The low gas velocity allowed to avoid significant pressure drop due to the relatively high ratio h/i.d. (=1.7), and low particle size (0.5–1.6 mm). The Reynolds number was 17.7 and corresponded to a laminar flow.

Three dry gas matrices (N_2, Air, Syngas) containing 200 ppmv of H_2S were used. This concentration of H_2S was representative to its level in real syngas [10]. The composition of the model syngas was selected based on literature data dealing with the gasification of various biomass and wastes. The model syngas was composed of realistic permanent gases concentrations: 30 v% of H_2, 39.98 v% of CO, 15 v% of CH_4 and 15 v% of CO_2 and 200 ppmv of H_2S. The Air matrix was composed of 78 v% of N_2, 21.98 v% of O_2 and 200 ppmv of H_2S. The gas passed through the char bed in an upstream flow at a flow rate of 0.18 L.min^{-1} which was controlled by a mass flow controller. To obtain the breakthrough curves, outlet gas composition was monitored using a μ-GC (My-GC, Agilent) and electrochemical cells (GasAlert Quattro, BW Technologies). Removal capacities Q_{remov} (in mg of H_2S removed/g of dry char) were calculated by applying Eq. (1):

$$Q_{remov} = \sum_{t_0}^{t_f} \left[Q_v . \left(C_0 - \frac{\Delta C_i}{2} \right) . 10^{-6} . \Delta t \right] . \frac{\rho_{H2S}}{m_{dry\ char}} \quad (1)$$

where Q_v is the total volumetric flow rate (L.min^{-1}), C_0 is the inlet gas H_2S concentration (200 ppmv), C_i is the outlet gas H_2S concentration (ppmv), ρ_{H2S} is the density of H_2S (g.L^{-1}), $m_{dry\ char}$ is the dry weight of char introduced in the column (g), and t_f is the bed saturation time (min). Removal capacities were determined when the adsorption bed was saturated, *i.e.* when the H_2S concentration at the bed outlet was equal to the inlet concentration (200 ppmv).

The chars recovered after H_2S removal tests were designed by adding the suffix "_gas matrix/H_2S" to their name.

First, a screening of the different chars was performed under the N_2 matrix. Then, the adsorption capacity of the two most efficient adsorbents was studied in the other gas matrices (Air and Syngas).

2.3. Characterization of the materials

The elemental composition of the chars (C, H, N, S content) was analyzed with a Thermo Finnigan AE1112 Series Flash. The O content was calculated by difference. The average data presented in this paper were obtained from at least six repetitions. The ash content of the parent feedstocks and chars was determined by measuring the residual mass after the combustion of 7.0 g of the sample (Nabertherm P330) at a temperature of 550 °C and 650 °C, respectively. At least three repetitions were performed for each sample.

The chemical composition at the overall scale of resulting ash was analyzed by X-ray fluorescence spectroscopy (XRFS) (SHIMADZU EDX-800HS). Compared to ICP-MS, the XRFS method allowed determining the chemical composition on a large sample (about 2 g against 20 mg with ICP-MS). The ash analysed was obtained from the combustion of around 20 g of each material. Thus, large samples representative of the materials were analysed, allowing to deal with the chemical heterogeneity of the waste.

Raman spectroscopy was used to determine the different carbonaceous structures of the chars. At least three areas (25 μm^2) of three particles of each material were analysed. A 10 bands deconvolution of the Raman spectra was performed with Matlab® in order to characterize the carbonaceous structure. The assignment of each band is presented in Table S1 [44].

The amount of acidic and basic O-containing groups on the char surface was measured using the Temperature Programmed Desorption method coupled with μ-GC (TPD-GC). Around 150 mg of char were introduced in a thermogravimetric analyser (Labsys T6 Evo) and heated from 30 to 1100 °C at a heating rate of 5 °C.min^{-1} under N_2 atmosphere. CO and CO_2 production was monitored by a μ-GC (My-GC, SRA Instruments). The decomposition of O-containing groups occurs at a given temperature and is accompanied by a release of CO or CO_2. Although the assignment of the different peaks during TPD analysis is still discussed in the literature, global trends have emerged in previous studies [40,45]. The correlations are given in (Table S2). The deconvolution of the experimental data, performed with Matlab®, was used to quantify the amount of CO or CO_2 released for each desorption peak. Thus, the different O-containing groups can be identified and quantified.

The characterization of the chars porosity was carried out using physical adsorption of N_2 at 77 K, after an outgassing step of 16 h under vacuum (1 mm Hg) at a temperature of 30 °C. The BET method was applied to determine the specific surface area of the chars (S_{BET}), and the methods HK and BJH were used to calculate the microporous and mesoporous volume, respectively. The average values presented in this article were obtained by at least three repetitions.

2.4. Characterization of sulfur compounds

The pH of the chars before and after the H_2S removal tests was measured by adding 0.4 g of dry char powder to 20 mL of distilled water. The suspension was stirred at least 24 h before measuring the pH of the suspension.

The chemical evolution of the char surface as well as the presence and the speciation of sulfur compounds were studied with Raman spectroscopy. A mapping of the surface of each material was performed by analysing 3 regions (of 25 μm^2) of two different particles. Thus, the results reflect the presence of sulfur products locally detected on the materials surface.

Thermogravimetric analysis device (ATG STA409PC, Netzsch) coupled with a mass spectrometer (OMNISTAR, Pfeiffer) were used to study the decomposition temperature of the different sulfur compounds, with the following settings: heating rate of 20 °C.min^{-1} up to 800 °C with a nitrogen flow rate of 3 L.h^{-1}. For each measurement, a sample of 200–300 mg of crushed char was analysed. The derivative thermogravimetric (DTG) curves were used for data analysis. The temperatures

Table 1
Elemental composition, pH_{pzc} and ash content of the materials.

Sample	Elemental analysis (wt%)					pH_{pzc}	Ash (wt%)	Ash composition (wt%)					
	C	H	N	S	O			CaO	Fe_2O_3	Al_2O_3	Cl	K_2O	P_2O_5
UWP	48.2	6.5	nd	nd	44.6	n.m	0.7	41.0	4.0	3.4	nd*	18.5	4.8
FW	40.9	5.8	7.4	nd	34.0	n.m	11.9	46.9	0.3	nd*	16.0	13.1	16.4
CFS	39.9	5.4	6.7	nd	30.5	n.m	17.5	17.9	0.9	42.4	0.6	4.5	27.2
c.UWP	87.2	1.8	0.6	nd	8.3	7.3	2.1	42.5	6.5	3.0	nd*	11.0	4.7
c.FW/CFS	44.1	1.3	3.1	nd	4.5	9.6	47.0	39.2	1.6	13.8	7.5	6.4	26.2
ox.UWP	84.3	1.8	0.7	nd	9.7	7.6	3.5	44.6	4.6	4.3	3.3	12.9	5.0
ox.FW/CFS	42.2	1.1	2.9	nd	7.8	9.6	45.9	42.5	0.8	14.3	9.5	6.7	19.9
ac.UWP	87.4	0.8	0.4	nd	8.9	9.0	2.5	42.2	3.6	2.0	nd*	13.2	4.2
ac.FW/CFS	32.6	0.9	1.4	nd	5.7	9.8	59.4	34.3	0.6	18.2	9.2	7.2	26.2

nd: not detected in the elemental analysis (< 0.2 wt%); nd*: not detected by XRF (< 0.001 wt%); n.m: not measured.

at which the mass losses were observed and the composition of the gas produced provided information on the nature of the sulfur compounds.

3. Results and discussion

3.1. Sorbents characterization

As textural and surface properties are expected to be involved in the H_2S removal efficiency of the chars, their physicochemical properties were characterized. Based on their elemental composition, two types of chars can be distinguished (Table 1). Chars from UWP were carbonaceous materials with low ash content (< 3.5 wt%), while FW/CFS-based chars were hybrid carbon-mineral materials with significantly high ash content (> 45 wt%). While the oxygenation process did not modify significantly the elemental composition of the chars, steam activation strongly increased the ash content of ac.FW/CFS (relative increase: 12.4 wt%) and decreased the carbon concentration (relative decrease: 11.5 wt%). This is explained by the gasification reaction of the carbonaceous matrix with steam catalysed by the mineral species of c.FW/CFS during the activation step [46].

The pH_{pzc} of the FW/CFS-based chars was significantly higher than that of UWP-based chars, and increased during the steam activation for both types of chars (Table 1). On the contrary, the oxygenation process did not significantly modify the pH of the chars. For all adsorbents, the pH_{pzc} was higher than 7.3, which is theoretically favorable for the fixation of acid gas such as H_2S.

Table 1 presents the ash composition of the chars measured by XRF. Calcium was the main mineral specie present in the ash of each char (< 34.3 wt%). The ashes of UWP-based chars were rich in Ca, K and Fe, while the ashes of FW/CFS-based chars had high contents of Ca, P, Al and Cl. A precise multi-scale characterization of the ashes of FW/CFS-based chars has been published in a previous article [47].

Table 2 shows that pyrolysis chars had specific surface area (S_{BET}) lower than 10 $m^2.g^{-1}$. The oxygenation process did not modify the porosity of the chars. However, the steam activation resulted in a large increase of the specific surface area of both materials. The S_{BET} of ac.UWP (625 $m^2.g^{-1}$) was more significantly increased than that of ac.FW/CFS (221 $m^2.g^{-1}$) during steam activation, due to its higher carbon content. The char ac.FW/CFS presented the largest mesoporous volume (0.099 $cm^3.g^{-1}$) which represented near 50% of the total porosity. On the contrary, ac.UWP contained mainly micropores. Its microporous volume represented 85% of the total pore volume. No workable adsorption isotherm could have been obtained with c.UWP, indicating that this method is not suitable for this kind of materials with low specific surface area [48] and relatively "unstable structure".

Temperature Programmed Desorption analysis indicated that FW/CFS-based chars had higher ratio of basic to acidic O- containing groups than UWP-based chars (Table 2). This property coupled with the larger amount of basic mineral species (such as Ca) can explain the higher pH_{pzc} of FW/CFS-based chars. The total amount of O-containing groups at the surface of ox.UWP increased during the oxygenation step (+40%), while it drastically decreased for ox.FW/CFS (−80%). It can be noted that c.FW/CFS presented a remarkably high content of O-containing groups compared to other chars. During the steam activation, the acidic groups were significantly removed from the char surface, leading to the increase of the ratio of basic to acidic groups (from 0.64 to 1.13 for UWP-based char, and from 2.14 to 6.80 for FW/CFS-based chars).

Data on the nature of the carbonaceous matrix obtained by Raman spectroscopy are given in Table 2. The ratio I_D/I_{tot} reflects the proportion of defects in graphene-like sheets, while the ratio $(I_D + I_G)/I_{tot}$ corresponds to the proportion of graphene-like structures (ordered structures) in the carbonaceous matrix. For UWP-based chars, the oxygenation and the steam activation increased the order of the carbonaceous structure ($(I_D + I_G)/I_{tot}$), and defects in graphene-like structures rose drastically during the steam activation (I_D/I_{tot} increased

Table 2
Textural properties (N_2 physical adsorption), amount of O-containing groups (TPD-μ-GC) and order of the carbonaceous matrix (Raman spectroscopy) of the different chars. (With S_{BET}: specific surface area, V_{micro}: microporous volume, V_{meso}: mesoporous volume; I_D/I_{tot}: large aromatic rings systems (≥6 rings) and imperfections in graphene-like sheets; $(I_D + I_G)/I_{tot}$: total graphene like structures).

Sample	S_{BET} ($m^2.g^{-1}$)	V_{micro} ($cm^3.g^{-1}$)	V_{meso} ($cm^3.g^{-1}$)	Basic groups ($mmol.g^{-1}$)	Acidic groups ($mmol.g^{-1}$)	I_D/I_{tot} (%)	$(I_D + I_G)/I_{tot}$ (%)
c.UWP	nd	nd	nd	0.11	0.17	22.2	49.6
c.FW/CFS	9.7	0.008	0.016	1.50	0.70	32.0	47.1
ox.UWP	78.8	0.032	0.021	0.11	0.27	21.8	53.7
ox.FW/CFS	9.0	0.004	0.026	0.32	0.12	28.9	46.0
ac.UWP	625.4	0.271	0.047	0.09	0.08	36.3	60.7
ac.FW/CFS	220.5	0.100	0.099	0.34	0.05	31.7	52.3

nd: not determined by N_2 adsorption; n.m: not measured.

Table 3
H_2S removal capacities of the different chars under dry nitrogen atmosphere.

Sample	c.UWP	c.FW/CFS	ox.UWP	ox.FW/CFS	ac.UWP	ac.FW/CFS
Q_{remov} ($mg_{H2S}.g^{-1}$)	0.04	0.22	1.81	0.12	12.92	66.60

from 49.6 to 60.7%). For FW/CFS-based chars, no clear evolution of the carbonaceous structure was observed during the modification processes, which was related to their low carbon content (Table 2).

3.2. H_2S removal tests in N_2 matrix

The purification efficiency of the different materials was firstly studied in a nitrogen gas matrix to evaluate the specific interactions between H_2S and the chars. Each test was repeated at least twice. The average removal capacities of the pyrolysis, oxygenated and activated chars are listed in Table 3. The pyrolysis chars had the lowest reactivity with removal capacities smaller than 0.22 $mg_{H2S}.g^{-1}$. The oxygenation step resulted in a slight improvement of the efficiency of ox.UWP, with a removal capacity of 1.81 $mg_{H2S}.g^{-1}$. On the contrary, the efficiency of ox.FW/CFS decreased by 45% after oxygenation. Steam activation remarkably improved the efficiency of the chars. The removal capacities reached 12.9 $mg_{H2S}.g^{-1}$ for ac.UWP, and 66.6 $mg_{H2S}.g^{-1}$ for ac.FW/CFS. In order to explain the different removal capacities of the chars, their physicochemical properties were investigated (Section 3.5).

The two steam activated chars proved that high H_2S removal capacities can be reached even under dry conditions. Indeed, the removal capacity of ac.UWP is comparable with that of other commercial activated carbons used under similar conditions (Xiao et al.: 9 $mg_{H2S}.g^{-1}$ [49]; Elsayed et al.: 5–31 $mg_{H2S}.g^{-1}$ [24]). Even if the dry conditions used in this article were detrimental to its efficiency compared to other studies performed in moist air [24,36,50–52], ac.FW/CFS was among the most efficient sludge-based chars produced without chemical additive for H_2S abatement with a removal capacity of 67 $mg_{H2S}.g^{-1}$.

A key point for the industrial use of sorbents is their regeneration capacity. Thermal regeneration of used activated chars was performed at 750 °C during 1.5 h under pure nitrogen. Then, the H_2S removal capacity of the regenerated chars was measured using the matrix N_2. On the one hand, the H_2S removal capacity of ac.UWP decreased by 20% after regeneration (from 13.0 to 10.3 $mg_{H2S}.g^{-1}$). On the other hand, ac.FW/CFS recovered its entire H_2S removal efficiency after the regeneration step (66.6 $mg_{H2S}.g^{-1}$). Thus, a simple thermal treatment allows to recover the initial efficiency of ac.FW/CFS. The two most efficient materials (ac.FW/CSF and ac.UWP) were then tested as H_2S adsorbents in two different dry gas matrices: Air and Syngas.

3.3. Effect of the gas composition on H_2S removal efficiency

The curves of the cumulative removal capacities of ac.UWP and ac.FW/CFS obtained with the different gas matrices are shown in Fig. 1. The gas composition had no notable impact on the removal capacity of ac.UWP which was almost stable at 12–13 $mg_{H2S}.g^{-1}$. Compared to the results obtained in N_2 matrix, the efficiency of ac.FW/CFS was almost unchanged in the Syngas matrix (66.6 versus 64.7 $mg_{H2S}.g^{-1}$, respectively). While previous studies showed that CO_2 had a detrimental effect on the biogas desulfurization efficiency of activated carbons [21,32], this result proved that no competitive adsorption occurred between the H_2S and the CO_2 from the syngas, which are two acid gases. This result was confirmed by the μ-GC analysis of the syngas at the fixed bed outlet during the H_2S removal tests. Indeed, the syngas composition at the outlet was strictly similar to the inlet composition, except for H_2S. However, the presence of O_2 in the dry Air matrix had a detrimental effect on the efficiency of ac.FW/CFS. Under Air matrix, its removal capacity decreased by 13.5 %. The speciation of the sulfur species after the H_2S removal tests was investigated to better understand the purification mechanisms and the effect of O_2 and Syngas on the purification efficiency of the activated chars.

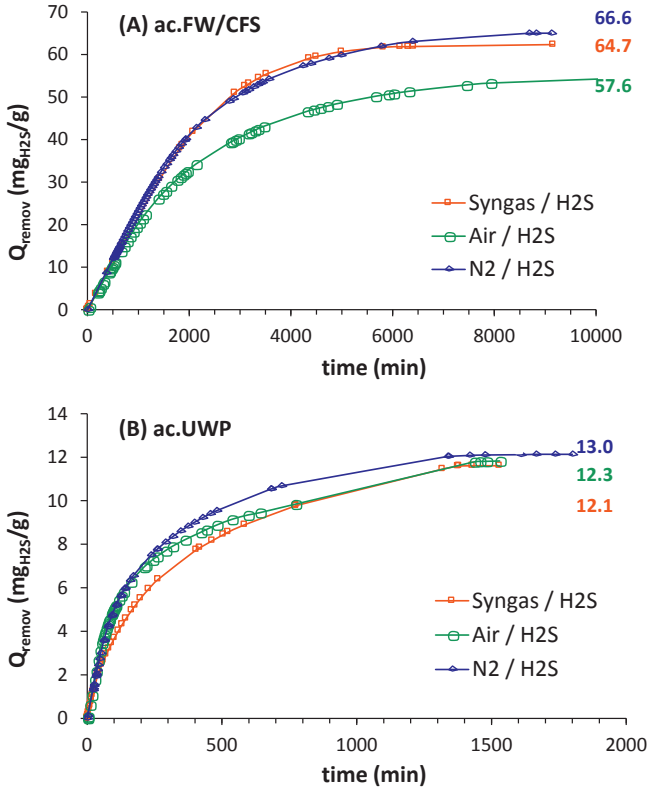

Fig. 1. Cumulative H_2S removal capacity in different dry gas matrices of (A) ac.FW/CFS, and (B) ac.UWP.

3.4. Effect of the gas composition on the sulfur species adsorbed

3.4.1. Evolution of the textural properties

The textural properties of ac.UWP were barely modified during the H_2S removal tests (Table 4), with a specific surface area (S_{BET}) almost constant at ≈600 $m^2.g^{-1}$. The pore size distribution of ac.UWP (Fig. 2-A) specified that the sulfur species were mainly localized in micropores higher than 4.5 Å. Contrary to ac.UWP, the specific surface area of ac.FW/CFS decreased significantly after H_2S removal tests (around 80% drop), which was explained by the higher amount of H_2S adsorbed by

Table 4
H_2S removal capacities of ac.UWP and ac.FW/CFS in the different gas matrices, and evolution of the textural properties and the pH after the H_2S removal tests.

Sample	Q_{remov} ($mg_{H2S}.g^{-1}$)	S_{BET} ($m^2.g^{-1}$)	V_{micro} ($cm^3.g^{-1}$)	V_{meso} ($cm^3.g^{-1}$)	pH (–)
ac.UWP	/	625.4	0.271	0.047	10.1
ac.UWP_N_2/H_2S	13.0	571.2	0.189	0.021	9.5
ac.UWP_Air/H_2S	12.3	596.6	0.198	0.017	9.0
ac.UWP_Syngas/H_2S	12.1	613.5	0.168	0.064	10.0
ac.FW/CFS	/	220.5	0.100	0.099	10.0
ac.FW/CFS_N_2/H_2S	66.6	39.4	0.004	0.066	8.4
ac.FW/CFS_Air/H_2S	57.6	35.5	0.000	0.049	7.8
ac.FW/CFS_Syngas/H_2S	64.7	40.3	0.001	0.055	8.1

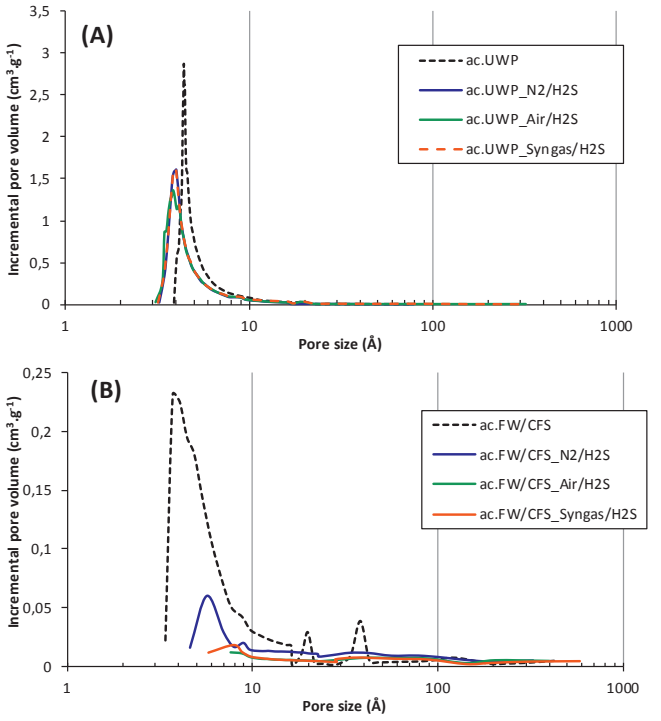

Fig. 2. Pore size distribution of (A) ac.UWP, and (B) ac.FW/CFS before and after the H_2S removal tests in different gas matrices. The distributions were obtained using the Horvath-Kawazoe (HK) and the BJH (Barrett, Joyner et Halenda) methods after N_2 adsorption/desorption tests at 77 K.

this material. The microporous volume of ac.FW/CFS was almost zero after the adsorption tests while the mesoporous volume reduced by ≈50% (Table 4). The pore size distribution of ac.FW/CFS (Fig. 2-B) showed that the sulfur products were concentrated in micropores lower than 10 Å, as well as in mesopores lower than 70 Å. The results are in agreement with the diameter of the H_2S molecule (1.9 Å). While micropores are described in the literature as important active sites [26,30,32], the mesopores lower than 70 Å appeared as important adsorption sites for H_2S in our study.

3.4.2. *Evolution of the pH*

During the H_2S removal tests, the pH of the chars decreased differently depending on the gas composition (Table 4). For both activated chars, the pH acidification was more important under the Air matrix than under other gas matrix. Indeed, the pH of the samples after the Air matrix tests decreased from 10.1 to 9.0 for ac.UWP, and from 10.0 to 7.8 for ac.FW/CFS. The pH decrease was more important for ac.FW/CFS than for ac.UWP, which could be explained by the higher reactivity of ac.FW/CFS. This result suggested that the presence of O_2 in the gas composition promoted the formation of acidic species leading to the acidification of the char surface. This acidification contributed to the decrease of the H_2S removal capacity of ac.FW/CFS under Air matrix.

However, the pH decrease was low compared to other values reported in the literature. For example, a study of *Bandosz* [53] showed that the pH of activated char from coconut shell used for H_2S removal from moist air decreased from 9.7 to 2.8. It can be concluded that the formation of sulfur oxide species is relatively low in our study.

3.4.3. *Identification of sulfur products using TGA-MS under N_2*

To go further in the identification of the sulfur species, TGA-MS coupling analyses were performed with fresh and used chars. Note that H_2S was the only sulfur-containing gas detected in the reactor effluent during the removal tests. Fig. 3 plots the derivative thermogravimetric (DTG) curves and the corresponding composition of the effluent gas as a function of the temperature. Based on the literature, the sulfur compounds desorption can occur in two temperature ranges, and the corresponding effluent gas composition provides information on the nature of these compounds [23,24,26]:

- In the first zone (plotted in grey in Fig. 3) between 200 and 350 °C, a SO_2 release indicates the desorption of physisorbed SO_2 or other sulfur oxides, while a H_2S release reveals the decomposition of metallic sulphides.
- In the second zone (plotted in pink in Fig. 3) between 350 and 600 °C: a release of SO_2 reflects the decomposition of sulfur radicals and/or elemental sulfur, while a release of H_2S indicates the decomposition of polysulfides.

The mass loss corresponding to each desorption peak was compared to the total amount of H_2S initially adsorbed on the char. Thus, the composition of the sulfur compounds adsorbed during the H_2S removal tests can be discussed.

For used ac.UWP after the tests in N_2 and syngas matrices, two mass losses appeared (black curves in Fig. 3-A). The first mass loss occurred at 285 °C and was related to a SO_2 release (blue curve), while the second appeared at 370 °C and was explained by a simultaneous release of H_2S (orange curve) and SO_2. Based on the literature data, this behavior indicated that the main sulfur products formed on ac.UWP during the H_2S removal tests under N_2 and Syngas matrices were sulfur oxide species and alkali metal sulfides (first mass loss). The second mass loss showed that sulfur radicals, elemental sulfur and/or polysulfides represented 20 wt% of the sulfur compounds under N_2, and 37 wt% under syngas matrix. The amount of physisorbed H_2S was negligible. For the tests with ac.UWP under the air matrix, only one mass loss appeared at 270 °C (Fig. 3-A), reflecting the formation of sulfur oxide species. Combined with the pH evolution, it can be concluded that the presence of O_2 in the gas matrix promoted the oxidation of H_2S to acidic species.

The thermal evolution of used ac.FW/CFS after the H_2S removal tests was dissimilar to that observed with used ac.UWP (Fig. 3-B). Whatever the gas matrix, three mass losses were observed at similar temperatures. The first one, observed at 250 °C, was higher for the tests performed under the Air matrix than for the other matrices (32 wt% of the total mass loss, versus 27 and 14 wt% in N_2 and Syngas, respectively). Combined with the pH evolution (Table 4), the promoting effect of O_2 on the H_2S oxidation to acidic species was confirmed. The second mass loss appeared between 340 and 530 °C and was associated with a release of H_2S (450 °C) and SO_2 (500 °C). This thermal evolution reflected the presence of sulfur radicals and/or elemental sulfur (SO_2 release), as well as polysulfides and/or metal sulfides (H_2S release). The release of SO_2 was superior to that of H_2S for all samples, even if the proportion of H_2S increased for ac.FW/CFS_Syngas/H_2S. Such a release of SO_2 and mass loss at a temperature slightly higher than the boiling point of elemental sulfur (446 °C) tends to demonstrate that H_2S was oxidized into elemental sulfur during the H_2S removal tests. This global mass loss represented 53% of the total mass loss of ac.FW/CFS after tests in N_2 and air matrices, and 61% in the syngas matrix. The third mass loss occurred at 600 °C and was characterized by a large release of CO_2 and small amounts of SO_2. This latter indicated the production of sulfur radicals, elemental sulfur, and/or metal sulfides during the H_2S removal tests. The sample ac.FW/CFS_Syngas/H_2S presented an additional mass loss at 730 °C with a release of SO_2, corresponding to elemental sulfur or metal sulfides. The total mass losses were close to the amount of H_2S captured by the material during the tests, and ranged from 5.5 to 6.0 wt%.

The characterizations evidenced that H_2S removal by the chars consisted in a complex adsorption-oxidation mechanism producing different sulfur species. To discriminate the presence of metal sulphide (S^{2-}) to that of sulfur oxide (S(+IV)) (both characterized by a mass loss at 200–350 °C and a release of SO_2), Raman spectroscopy was used.

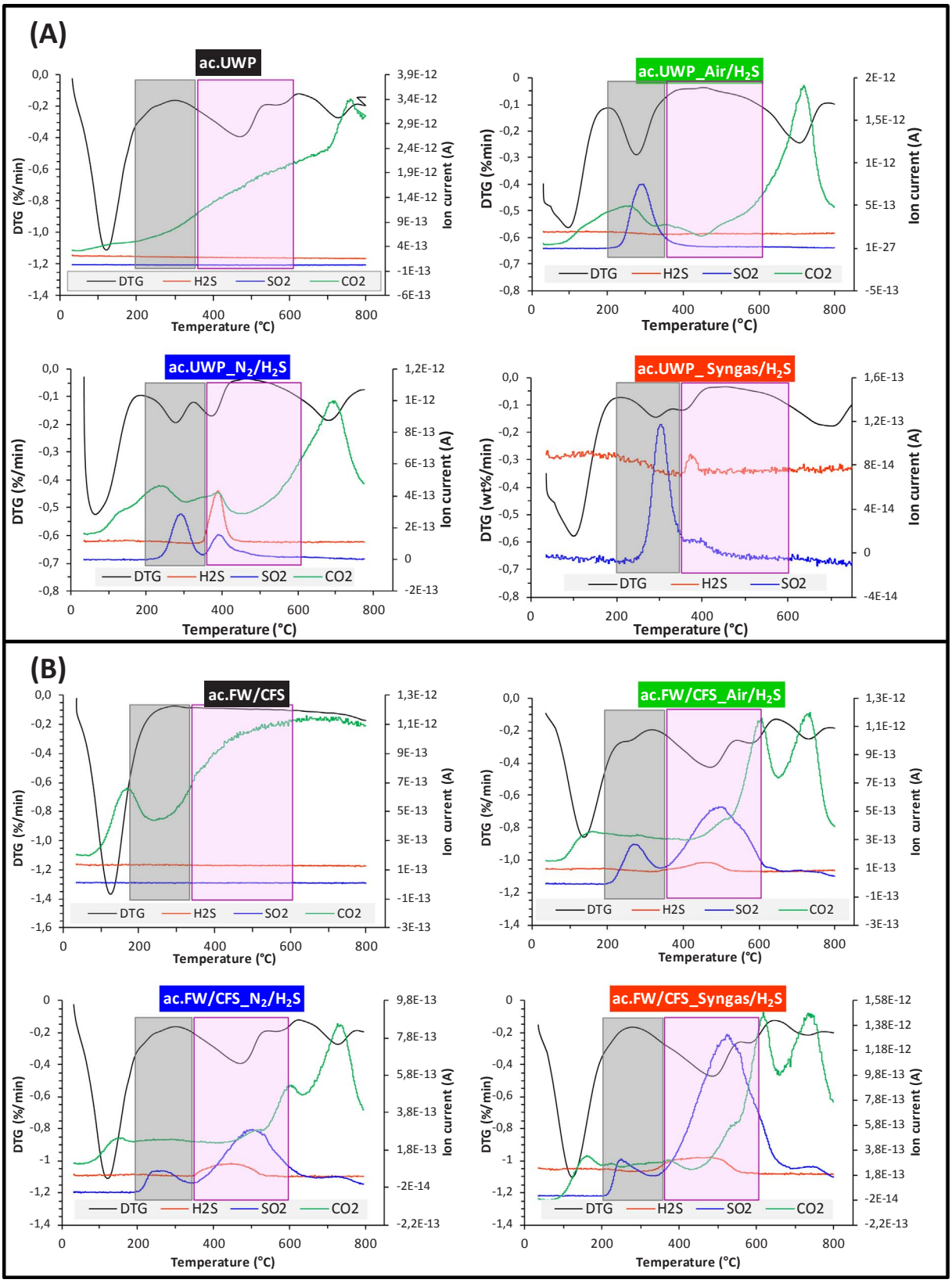

Fig. 3. TGA-MS analysis of ac.UWP (A) and ac.FW/CFS (B) before and after the H_2S removal tests in different gas matrices.

3.4.4. Identification of sulfur products using Raman spectroscopy

Raman analysis showed that no area rich in sulfur species was observed at the surface of ac.UWP_N_2/H_2S. After the test in syngas matrix, two different mineral spectra were observed on the surface of ac.UWP_Syngas/H_2S (Fig. 4-A). The first Raman spectrum (ac.UWP_Syngas/H_2S_1) displayed peaks at 420 and 610 cm^{-1}, while the second (ac.UWP_Syngas/H_2S_2) had only one peak at 340 cm^{-1}. The comparison with the RRUFF database [54] revealed that these peaks resulted

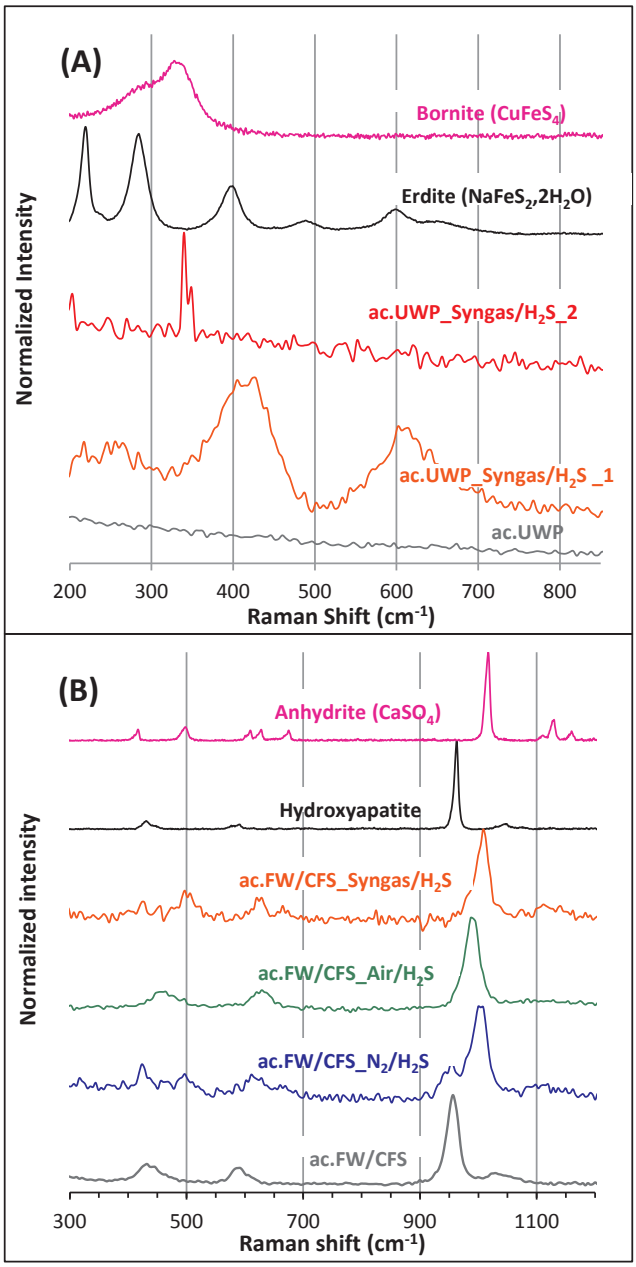

Fig. 4. Normalized Raman spectra of (A) ac.UWP, and (B) ac.FW/CFS before and after the H_2S removal tests. Experimental spectra were compared with the RRUFF database spectra in order to identify the sulfur species formed.

from the presence of minerals containing a Fe-S bond, such as Erdite ($NaFeS_2{\cdot}2H_2O$) and Bornite (Cu_5FeS_4). Thus, the 3.6 wt% of Fe present in the ac.UWP ashes (Table 2) locally promoted the H_2S removal through the formation of iron sulfides. Previous studies reported the important role of iron in the H_2S removal capacity of several sorbents [20,55,56]. Recently, small amount of copper was proved to increase the reactivity of ZnO for H_2S adsorption [21]. The traces of copper in the ac.UWP ashes (< 0.7 wt%) could have promoted the interactions between H_2S and the iron particles of this char.

The surface mapping of ac.FW/CFS after the H_2S removal tests revealed a single type of mineral spectrum, whatever the gas matrix used for the H_2S removal tests. This spectrum had peaks at 495, 620, 960, 1010 and 1115 cm^{-1} (Fig. 4-B). The peak observed at 960 cm^{-1} was also present on the spectrum of ac.FW/CFS before the tests. This peak matched with the hydroxyapatite phase ($Ca_5(PO_4)_3(OH)$), as detailed elsewhere [47]. The other peaks testified to the presence of an anhydrous calcium sulphate named Anhydrite ($CaSO_4$). These results were in agreement with the ash composition of ac.FW/CFS, in which the calcium was the main mineral specie (Table 2).

3.5. Influence of the physicochemical properties of the chars on their H_2S removal capacity

The large amount of ash (> 45.9 wt%) and active mineral species in the composition of FW/CFS-based chars can contribute to their high H_2S removal efficiency compared to UWP-based chars. These results are in agreement with previous studies which reported that mineral species react with H_2S to form metal sulfides species [23,25]. Despite its low ash content (2.5 wt%), the presence of iron and copper in the ash composition of ac.UWP promoted its adsorption capacity by the formation of iron sulfide species (Fig. 4-A). Calcium was the main mineral specie in FW/CFS-based chars and was proved to be present in the form of hydroxyapatite and small calcium oxide particles (1–10 μm) which were well dispersed on the char surface [47]. Original results obtained with Raman spectroscopy showed that the calcium-containing particles contributed to the high H_2S removal capacity of ac.FW/CFS with the formation of calcium sulphate $CaSO_4$ (Fig. 4-B). Oxidation reactions of H_2S were proved to occur even under dry N_2 and syngas matrix.

The higher pH alkalinity contributed to the higher treatment capacity of FW/CFS-based chars compared to UWP-based char (Table 1). Indeed, alkaline pH can promote the adsorption of acid gases, such as H_2S [26]. The increase of the pH_{pzc} after the steam activation was expected to contribute to the large increase of the activated char's performances. However, the pH_{pzc}, the ash content and the mineral composition were not sufficient to understand the removal capacity of the different chars. For example, c.FW/CFS had higher pH_{pzc} and ash content than ac.UWP (respectively 9.6 vs 9.0, and 47.0 vs 2.5 wt%), but lower H_2S removal performance in N_2 matrix (0.22 vs 12.92 $mg_{H2S}.g^{-1}$, respectively). Thus, textural properties, O-containing groups and the nature of the carbonaceous matrix were investigated to explain these results.

The specific surface area appeared as a key property for the removal capacity of the chars [13]. Activated and oxygenated chars had comparable chemical properties (composition, metals in the oxide form) but significantly different S_{BET}. The high S_{BET} of activated chars resulted in a tremendous increase of their H_2S removal capacity. This is explained by a better dispersion of the minerals on the surface, and by a faster diffusion of the H_2S molecules from the gas to the adsorption sites. While micropores are described in the literature as active sites for H_2S adsorption [26,30,32], mesopores lower than 70 Å were identified in this study as important adsorption sites (Fig. 2). The increase of pH_{pzc} and of defects in graphene-like structures (for ac.UWP) could also contribute to the higher efficiency of activated chars.

Due to their interaction with the acid gas H_2S, the basic surface groups (quinone, lactone, ether) contributed to the char performances. The total amount of O-containing groups at the surface of ox.UWP increased during the oxygenation step (+40%), while it drastically decreased for ox.FW/CFS (−80%). As pyrolysis chars and oxygenated chars had comparable S_{BET}, the decrease of the removal capacity of ox.FW/CFS (from 0.22 $mg_{H2S}.g^{-1}$ to 0.12 $mg_{H2S}.g^{-1}$) and the increase of ox.UWP efficiency (from 0.04 to 1.81 $mg_{H2S}.g^{-1}$) were mainly explained by the evolution of the O-containing groups. During the steam activation, the thermal effect significantly removed the acidic groups, leading to the increase of the ratio of basic to acidic groups on the activated chars surface (from 0.64 to 1.13 for UWP-based char, and from 2.14 to 6.80 for FW/CFS-based chars). This increase contributed to promote the H_2S removal efficiency of activated chars. Despite the large amount of O-containing groups on the surface of c.FW/CFS (2.2 $mmol.g^{-1}$), its H_2S removal capacity was low (0.22 $mg_{H2S}.g^{-1}$). This observation showed that the isolated effect of O-containing groups on the adsorption capacity was relatively low.

Raman spectroscopy evidenced that defects in graphene-like

structures rose drastically during the steam activation of ac.UWP (I_D/I_{tot} increased from 49.6 to 60.7%). These structures are known to be active sites for H_2S adsorption [57] and contributed to the high removal capacity of ac.UWP.

The two pyrolysis chars had significantly different physicochemical properties which were simultaneously modified during oxygenation and steam activation processes. For this reason, it is difficult to discriminate the individual contribution of each property in the H_2S removal capacity of the chars. However, the results showed that the important char properties for H_2S removal are: high specific surface area and mesoporous volume, alkaline pH surface, presence of mineral species on the surface (especially Ca, Al, Fe), O-containing groups (especially basic groups), and disorganized carbonaceous structure. The combined effect of these properties explained the high H_2S removal capacity of the activated chars, especially ac.FW/CFS. In fact, ac.FW/CFS had the highest pH_{pzc}, the highest ash content, the lowest density of acidic groups and high density of basic groups, the highest mesoporous volume, and a significant S_{BET} of 220.5 $m^2.g^{-1}$, which explain its highest H_2S removal capacity

4. Discussion: mechanisms of H_2S removal by chars

The complete characterization of the char's properties and the identification of the sulfur compounds adsorbed evidenced that the retention process of H_2S on the char surface consists of a complex reaction mechanism involving the physicochemical properties of the chars and the gas composition. In addition, H_2S was proved to be oxidized even under dry N_2 and Syngas matrix. Based on these results, the following reactions proposed are expected to occur in the H_2S retention mechanism.

First, the H_2S molecule can be physisorbed on active sites (named "*") at the char surface, according to Eq. (2). However, the TGA-MS analyses proved that this reaction was negligible in our study.

$$H_2S_{(g)} + * \leftrightarrow H_2S_{(ads)} \quad (2)$$

The initial humidity of the chars or the water generated by Eq. (4)–(6) can dissociate the H_2S (Eq. (3)):

$$H_2S \leftrightarrow^{K_{\alpha 1}} H^+ + HS^- \leftrightarrow^{K_{\alpha 2}} 2H^+ + S^{2-} \quad (3)$$

With $K_{\alpha 1} = 10^{-7}$ and $K_{\alpha 2} = 10^{-13}$: the H_2S acidity constants for the first and second dissociation.

The metal oxide species inherently contained in the ashes of the chars reacted with H_2S to produce metal sulfides (Eq. (4)). Further oxidation of the metal sulfur with oxygenated organic and inorganic species led to the formation of metal sulphate.

$$xH_2S_{(g)} + MeO_x \leftrightarrow MeS_x + xH_2O \quad (4)$$

The O-containing groups also increased the H_2S removal capacity of the chars, by the substitution reaction (Eq. (5)) and the H_2S oxidation reaction (Eq. (6)):

$$C(O) + H_2S_{(g)} \leftrightarrow C(S) + H_2O \quad (5)$$

$$C(O) + H_2S_{(g)} \leftrightarrow C_{free} + S_{(sol)} + SO_x + H_2O \quad (6)$$

The presence of metal oxide particles and O-containing groups on the char surface explained the oxidation reactions of H_2S under dry N_2 and Syngas matrix.

The defects in graphene-like sheets characterized with Raman spectroscopy can provide free carbon sites (C_{free}) reacting with H_2S according to Eqs. (7) and (8):

$$C_{free} + H_2S_{(g)} \leftrightarrow C(H_2S)_{ads} \quad (7)$$

$$C(H_2S)_{ads} + H_2S_{(g)} \leftrightarrow C(S_xH_y)_{ads} \quad (8)$$

In the presence of Air, the important acidification of the surface can be explained by the oxidation of H_2S (Eq. (9)):

$$H_2\ S + 2O_2 \leftrightarrow H_2SO_4 \quad (9)$$

5. Conclusions

This article investigated the valorization of waste-based chars as sorbents for H_2S removal from syngas. Two chars were produced by the pyrolysis of: (1) used wood pallets (UWP), and (2) a 50/50% mixture of food waste (FW) and coagulation-flocculation sludge (CFS). The chars were modified by low-cost and eco-friendly processes without chemicals: gas phase oxygenation at 280 °C and steam activation at 850 °C. The H_2S removal tests were performed at ambient temperature under various dry matrix (N_2, Air, Syngas) to study the effect of the gas composition on the adsorption efficiency. To the best of our knowledge, the use of char for H_2S removal from syngas at ambient temperature had never been studied previously.

The screening in N_2 matrix evidenced that steam activation remarkably increased the H_2S removal capacity of the activated chars ac.FW/CFS and ac.UWP. Elemental analysis, XRF, N_2 adsorption, TPD-μ-GC and Raman spectroscopy revealed that the important char properties for H_2S removal are: high specific surface area and mesoporous volume, alkaline pH surface, presence of mineral species on the surface (especially Ca, Al, Fe), O-containing groups (especially basic groups), and disorganized carbonaceous structure. While micropores are described in the literature as active sites for H_2S adsorption, mesopores lower than 70 Å were identified in this study as important adsorption sites. Under dry N_2 matrix, the sorbent ac.FW/CFS was the most efficient material for H_2S abatement with a removal capacity of 67 $mg_{H2S}.g^{-1}$. The performance of this char is competitive with the most efficient activated carbons produced without chemical additives and used under more favorable conditions (moist air).

The presence of oxygen in the dry Air matrix decreased the adsorption capacity of ac.FW/CFS, due to the formation of acidic sulfur species. The acidification of the char surface explained the decrease of its H_2S removal capacity (from 67 to 57 $mg_{H2S}.g^{-1}$). Under dry Syngas matrix, ac.FW/CFS remained efficient and selective toward H_2S abatement despite the presence of another acid gas (CO_2). In addition, a simple thermal regeneration under nitrogen flow allowed a complete regeneration of the initial removal capacity of this activated char, and extended its utilization span.

Sulfur compounds speciation was studied with pH measurements, TGA-MS, and Raman spectroscopy. The results highlighted the large variety of sulfur compounds produced during the H_2S removal tests, resulting from a complex reaction mechanism involving the physicochemical properties of the chars and the operating conditions.

In line with the need to develop a circular economy, this study provided promising results toward the *in-situ* valorization of waste-based chars in the pyrogasification process as efficient, low-cost, and eco-friendly adsorbents for H_2S removal from syngas.

Acknowledgement

The authors gratefully acknowledge the ANR Carnot M.I.N.E.S. for financial support (CHARPURGAS grant 30530). The authors also thank Alain Thorel, Anthony Chesnaud, Sarah Berhanu, Céline Boachon, Laurène Haurie, Mickaël Ribeiro, Pierre Bertorelle and Denis Marty for help with experiments.

Appendix A. Supplementary data

Supplementary data associated with this article can be found, in the online version, at http://dx.doi.org/10.1016/j.cej.2017.11.162.

References

[1] D. Czajczyńska, L. Anguilano, H. Ghazal, R. Krzyżyńska, A.J. Reynolds, N. Spencer,

H. Jouhara, Potential of pyrolysis processes in the waste management sector, Therm. Sci. Eng. Prog. 3 (2017) 171–197, http://dx.doi.org/10.1016/j.tsep.2017.06.003.
[2] C. Di Blasi, Modeling chemical and physical processes of wood and biomass pyrolysis, Prog. Energy Combust. Sci. 34 (2008) 47–90, http://dx.doi.org/10.1016/j.pecs.2006.12.001.
[3] R. Zhao, N. Coles, Z. Kong, J. Wu, Effects of aged and fresh biochars on soil acidity under different incubation conditions, Soil Tillage Res. 146 (Part B) (2015) 133–138, http://dx.doi.org/10.1016/j.still.2014.10.014.
[4] M.M. Diémé, M. Hervy, S.N. Diop, C. Gérente, A. Villot, Y. Andres, C.K. Diawara, Sustainable conversion of agriculture and food waste into activated carbons devoted to fluoride removal from drinking water in senegal, Int. J. Chem. 8 (2015) 8, http://dx.doi.org/10.5539/ijc.v8n1p8.
[5] L. Sigot, M. Fontseré Obis, H. Benbelkacem, P. Germain, G. Ducom, Comparing the performance of a 13X zeolite and an impregnated activated carbon for H_2S removal from biogas to fuel an SOFC: influence of water, Int. J. Hydrogen Energy 41 (2016) 18533–18541, http://dx.doi.org/10.1016/j.ijhydene.2016.08.100.
[6] M. Hervy, C. Gérente, A. Villot, L. Le Coq, E. Weiss-Hortala, D. Pham Minh, A. Nzihou, Recycling of pyrolysis chars from food waste, wastewater treatment sludge and wood in the syngas purification, in: Proc. Int. Conf. Solid Waste – Knowl. Transf. Sustain. Resour. Manag., J.W.C. Wong, M. Nelles, R. D. Tyagi and A. Selvam, 2015.
[7] F. Nestler, L. Burhenne, M.J. Amtenbrink, T. Aicher, Catalytic decomposition of biomass tars: the impact of wood char surface characteristics on the catalytic performance for naphthalene removal, Fuel Process. Technol. 145 (2016) 31–41, http://dx.doi.org/10.1016/j.fuproc.2016.01.020.
[8] Y. Shen, M. Chen, T. Sun, J. Jia, Catalytic reforming of pyrolysis tar over metallic nickel nanoparticles embedded in pyrochar, Fuel 159 (2015) 570–579, http://dx.doi.org/10.1016/j.fuel.2015.07.007.
[9] P.J. Woolcock, R.C. Brown, A review of cleaning technologies for biomass-derived syngas, Biomass Bioenergy 52 (2013) 54–84, http://dx.doi.org/10.1016/j.biombioe.2013.02.036.
[10] R.P. Gupta, B.S. Turk, J.W. Portzer, D.C. Cicero, Desulfurization of syngas in a transport reactor, Environ. Prog. 20 (2001) 187–195, http://dx.doi.org/10.1002/ep.670200315.
[11] A. Bassani, G. Bozzano, C. Pirola, E. Ranzi, S. Pierucci, F. Manenti, Low impact methanol production from sulfur rich coal gasification, Energy Procedia 105 (2017) 4519–4524, http://dx.doi.org/10.1016/j.egypro.2017.03.970.
[12] L. Sigot, G. Ducom, P. Germain, Adsorption of hydrogen sulfide (H_2S) on zeolite (Z): retention mechanism, Chem. Eng. J. 287 (2016) 47–53, http://dx.doi.org/10.1016/j.cej.2015.11.010.
[13] T.J. Bandosz, Effect of pore structure and surface chemistry of virgin activated carbons on removal of hydrogen sulfide, Carbon 37 (1999) 483–491.
[14] M. Hussain, N. Abbas, D. Fino, N. Russo, Novel mesoporous silica supported ZnO adsorbents for the desulphurization of biogas at low temperatures, Chem. Eng. J. 188 (2012) 222–232, http://dx.doi.org/10.1016/j.cej.2012.02.034.
[15] X. Wang, T. Sun, J. Yang, L. Zhao, J. Jia, Low-temperature H2S removal from gas streams with SBA-15 supported ZnO nanoparticles, Chem. Eng. J. 142 (2008) 48–55, http://dx.doi.org/10.1016/j.cej.2007.11.013.
[16] S. Li, K. Li, J. Hao, P. Ning, L. Tang, X. Sun, Acid modified mesoporous Cu/SBA-15 for simultaneous adsorption/oxidation of hydrogen sulfide and phosphine, Chem. Eng. J. 302 (2016) 69–76, http://dx.doi.org/10.1016/j.cej.2016.05.037.
[17] H.S. Song, M.G. Park, W. Ahn, S.N. Lim, K.B. Yi, E. Croiset, Z. Chen, S.C. Nam, Enhanced adsorption of hydrogen sulfide and regeneration ability on the composites of zinc oxide with reduced graphite oxide, Chem. Eng. J. 253 (2014) 264–273, http://dx.doi.org/10.1016/j.cej.2014.05.058.
[18] H.S. Song, M.G. Park, E. Croiset, Z. Chen, S.C. Nam, H.-J. Ryu, K.B. Yi, Effect of active zinc oxide dispersion on reduced graphite oxide for hydrogen sulfide adsorption at mid-temperature, Appl. Surf. Sci. 280 (2013) 360–365, http://dx.doi.org/10.1016/j.apsusc.2013.04.161.
[19] M. Florent, T.J. Bandosz, Effects of surface heterogeneity of cobalt oxyhydroxide/graphite oxide composites on reactive adsorption of hydrogen sulfide, Microporous Mesoporous Mater. 204 (2015) 8–14, http://dx.doi.org/10.1016/j.micromeso.2014.11.001.
[20] S. Stita, M. Galera Martínez, H. Pham Xuan, D. Pham Minh, A. Nzihou, P. Sharrock, Metal-doped apatitic calcium phosphates: preparation, characterization, and reactivity in the removal of hydrogen sulfide from gas phase, Compos. Interfaces 22 (2015) 503–515, http://dx.doi.org/10.1080/09276440.2015.1049096.
[21] M. Balsamo, S. Cimino, G. de Falco, A. Erto, L. Lisi, ZnO-CuO supported on activated carbon for H2S removal at room temperature, Chem. Eng. J. 304 (2016) 399–407, http://dx.doi.org/10.1016/j.cej.2016.06.085.
[22] S.P. Hernández, M. Chiappero, N. Russo, D. Fino, A novel ZnO-based adsorbent for biogas purification in H2 production systems, Chem. Eng. J. 176 (2011) 272–279, http://dx.doi.org/10.1016/j.cej.2011.06.085.
[23] A. Bagreev, T.J. Bandosz, On the mechanism of hydrogen sulfide removal from moist air on catalytic carbonaceous adsorbents, Ind. Eng. Chem. Res. 44 (2005) 530–538, http://dx.doi.org/10.1021/ie049277o.
[24] Y. Elsayed, M. Seredych, A. Dallas, T.J. Bandosz, Desulfurization of air at high and low H_2S concentrations, Chem. Eng. J. 155 (2009) 594–602, http://dx.doi.org/10.1016/j.cej.2009.08.010.
[25] L.M.L. Leuch, A. Subrenat, P.L. Cloirec, Hydrogen sulfide and ammonia removal on activated carbon fiber cloth-supported metal oxides, Environ. Technol. 26 (2005) 1243–1254, http://dx.doi.org/10.1080/09593332608618594.
[26] F. Adib, A. Bagreev, T.J. Bandosz, Effect of pH and surface chemistry on the mechanism of H_2S removal by activated carbons, J. Colloid Interface Sci. 216 (1999) 360–369.
[27] J. Guo, Y. Luo, A.C. Lua, R. Chi, Y. Chen, X. Bao, S. Xiang, Adsorption of hydrogen sulphide (H_2S) by activated carbons derived from oil-palm shell, Carbon 45 (2007) 330–336, http://dx.doi.org/10.1016/j.carbon.2006.09.016.
[28] J. Köchermann, J. Schneider, S. Matthischke, S. Rönsch, Sorptive H_2S removal by impregnated activated carbons for the production of SNG, Fuel Process. Technol. 138 (2015) 37–41, http://dx.doi.org/10.1016/j.fuproc.2015.05.004.
[29] R. Yan, T. Chin, Y.L. Ng, H. Duan, D.T. Liang, J.H. Tay, Influence of surface properties on the mechanism of H_2S removal by alkaline activated carbons, Environ. Sci. Technol. 38 (2004) 316–323, http://dx.doi.org/10.1021/es0303992.
[30] T. Mochizuki, M. Kubota, H. Matsuda, L.F. D'Elia Camacho, Adsorption behaviors of ammonia and hydrogen sulfide on activated carbon prepared from petroleum coke by KOH chemical activation, Fuel Process. Technol. 144 (2016) 164–169, http://dx.doi.org/10.1016/j.fuproc.2015.12.012.
[31] C. Huang, C. Chen, S. Chu, Effect of moisture on H_2S adsorption by copper impregnated activated carbon, J. Hazard. Mater. 136 (2006) 866–873, http://dx.doi.org/10.1016/j.jhazmat.2006.01.025.
[32] E. Sisani, G. Cinti, G. Discepoli, D. Penchini, U. Desideri, F. Marmottini, Adsorptive removal of H_2S in biogas conditions for high temperature fuel cell systems, Int. J. Hydrogen Energy 39 (2014) 21753–21766, http://dx.doi.org/10.1016/j.ijhydene.2014.07.173.
[33] D. Nguyen-Thanh, T.J. Bandosz, Activated carbons with metal containing bentonite binders as adsorbents of hydrogen sulfide, Carbon 43 (2005) 359–367, http://dx.doi.org/10.1016/j.carbon.2004.09.023.
[34] Y. Feng, J. Dou, A. Tahmasebi, J. Xu, X. Li, J. Yu, F. Yin, Regeneration of Fe–Zn–Cu sorbents supported on activated lignite char for the desulfurization of coke oven gas, Energy Fuels 29 (2015) 7124–7134, http://dx.doi.org/10.1021/acs.energyfuels.5b01909.
[35] T.J. Bandosz, A. Bagreev, F. Adib, A. Turk, Unmodified versus caustics-impregnated carbons for control of hydrogen sulfide emissions from sewage treatment plants, Environ. Sci. Technol. 34 (2000) 1069–1074, http://dx.doi.org/10.1021/es9813212.
[36] A. Ros, M.A. Montes-Moran, E. Fuente, D.M. Nevskaia, M.J. Martin, Dried sludges and sludge-based chars for H_2S removal at low temperature: influence of sewage sludge characteristics, Environ. Sci. Technol. 40 (2006) 302–309, http://dx.doi.org/10.1021/es050996j.
[37] L. Haeusler, G. Berthoin, ADEME-Déchets-edition 2015, (2015). http://www.ademe.fr/dechets-chiffres-cles.
[38] A.K. Gupta, S. Ibrahim, A. Al Shoaibi, Advances in sulfur chemistry for treatment of acid gases, Prog. Energy Combust. Sci. 54 (2016) 65–92, http://dx.doi.org/10.1016/j.pecs.2015.11.001.
[39] E. Mura, O. Debono, A. Villot, F. Paviet, Pyrolysis of biomass in a semi-industrial scale reactor: study of the fuel-nitrogen oxidation during combustion of volatiles, Biomass Bioenergy 59 (2013) 187–194, http://dx.doi.org/10.1016/j.biombioe.2013.09.001.
[40] M. Ducousso, E. Weiss-Hortala, A. Nzihou, M.J. Castaldi, Reactivity enhancement of gasification biochars for catalytic applications, Fuel 159 (2015) 491–499, http://dx.doi.org/10.1016/j.fuel.2015.06.100.
[41] M. Molina-Sabio, M.T. Gonzalez, F. Rodriguez-Reinoso, A. Sepúlveda-Escribano, Effect of steam and carbon dioxide activation in the micropore size distribution of activated carbon, Carbon 34 (1996) 505–509, http://dx.doi.org/10.1016/0008-6223(96)00006-1.
[42] N. Mohamad Nor, L.C. Lau, K.T. Lee, A.R. Mohamed, Synthesis of activated carbon from lignocellulosic biomass and its applications in air pollution control—a review, J. Environ. Chem. Eng. 1 (2013) 658–666, http://dx.doi.org/10.1016/j.jece.2013.09.017.
[43] P. Le Cloirec, Adsorption en traitement de l'air, Technique et documentation, Londres; Paris; New-York, 2003.
[44] M. Asadullah, S. Zhang, Z. Min, P. Yimsiri, C.-Z. Li, Effects of biomass char structure on its gasification reactivity, Bioresour. Technol. 101 (2010) 7935–7943, http://dx.doi.org/10.1016/j.biortech.2010.05.048.
[45] J.-H. Zhou, Z.-J. Sui, J. Zhu, P. Li, D. Chen, Y.-C. Dai, W.-K. Yuan, Characterization of surface oxygen complexes on carbon nanofibers by TPD, XPS and FT-IR, Carbon 45 (2007) 785–796, http://dx.doi.org/10.1016/j.carbon.2006.11.019.
[46] C. Dupont, S. Jacob, K.O. Marrakchy, C. Hognon, M. Grateau, F. Labalette, D. Da Silva Perez, How inorganic elements of biomass influence char steam gasification kinetics, Energy 109 (2016) 430–435, http://dx.doi.org/10.1016/j. energy.2016.04.094.
[47] M. Hervy, S. Berhanu, E. Weiss-Hortala, A. Chesnaud, C. Gérente, A. Villot, D. Pham Minh, A. Thorel, L. Le Coq, A. Nzihou, Multi-scale characterisation of chars mineral species for tar cracking, Fuel 189 (2017) 88–97, http://dx.doi.org/10.1016/j.fuel.2016.10.089.
[48] K.S. Sing, D. Everett, R.A. Haul, L. Moscou, R. Pierotti, J. Rouquerol, T. Siemieniewska, Reporting physisorption data for gas/solid systems with special reference to the determination of surface area and porosity, Pure Appl. Chem. 57 (1985) 603–619.
[49] X. Xiao, D.D. Le, L. Li, X. Meng, J. Cao, K. Morishita, T. Takarada, Catalytic steam gasification of biomass in fluidized bed at low temperature: conversion from livestock manure compost to hydrogen-rich syngas, Biomass Bioenergy 34 (2010) 1505–1512, http://dx.doi.org/10.1016/j.biombioe.2010.05.001.
[50] M. Seredych, C. Strydom, T.J. Bandosz, Effect of fly ash addition on the removal of hydrogen sulfide from biogas and air on sewage sludge-based composite adsorbents, Waste Manage. 28 (2008) 1983–1992, http://dx.doi.org/10.1016/j.wasman.2007.08.020.
[51] R. Wallace, M. Seredych, P. Zhang, T.J. Bandosz, Municipal waste conversion to hydrogen sulfide adsorbents: investigation of the synergistic effects of sewage sludge/fish waste mixture, Chem. Eng. J. 237 (2014) 88–94, http://dx.doi.org/10.

1016/j.cej.2013.10.005.
[52] Y. Xiao, S. Wang, D. Wu, Q. Yuan, Catalytic oxidation of hydrogen sulfide over unmodified and impregnated activated carbon, Sep. Purif. Technol. 59 (2008) 326–332, http://dx.doi.org/10.1016/j.seppur.2007.07.042.
[53] T.J. Bandosz, On the adsorption/oxidation of hydrogen sulfide on activated carbons at ambient temperatures, J. Colloid Interface Sci. 246 (2002) 1–20, http://dx.doi.org/10.1006/jcis.2001.7952.
[54] R.T. Downs, The RRUFF Project: an integrated study of the chemistry, crystallography, Raman and infrared spectroscopy of minerals., Program Abstr. 19th Gen. Meet. Int. Mineral. Assoc. Kobe Jpn. O03-13. (n.d.).
[55] A. Bagreev, S. Bashkova, D.C. Locke, T.J. Bandosz, Sewage sludge-derived materials as efficient adsorbents for removal of hydrogen sulfide, Environ. Sci. Technol. 35 (2001) 1537–1543, http://dx.doi.org/10.1021/es001678h.
[56] A. Bagreev, T.J. Bandosz, Efficient hydrogen sulfide adsorbents obtained by pyrolysis of sewage sludge derived fertilizer modified with spent mineral oil, Environ. Sci. Technol. 38 (2004) 345–351, http://dx.doi.org/10.1021/es0303438.
[57] W. Feng, S. Kwon, E. Borguet, R. Vidic, Adsorption of hydrogen sulfide onto activated carbon fibers: effect of pore structure and surface chemistry, Environ. Sci. Technol. 39 (2005) 9744–9749, http://dx.doi.org/10.1021/es0507158.